Journal of Food Engineering 104 (2011) 548–556

Contents lists available at ScienceDirect

Journal of Food Engineering

journal homepage: www.elsevier.com/locate/jfoodeng

Analysis of radio frequency (RF) power distribution in dry food materials

G. Tiwari [a], S. Wang [a], J. Tang [a,*], S.L. Birla [b]

[a] Department of Biological Systems Engineering, Washington State University, Pullman, WA 99164-6120, USA
[b] Department of Biological Systems Engineering, University of Nebraska, Lincoln, NE 68583, USA

ARTICLE INFO

Article history:
Received 8 May 2010
Received in revised form 13 January 2011
Accepted 15 January 2011
Available online 21 January 2011

Keywords:
Radio frequency
Computer simulation
Dielectric properties
Power uniformity index

ABSTRACT

The objectives of this research were to investigate the influence of various factors on radio frequency (RF) power distribution in dry food materials, placed in a 12 kW, 27.12 MHz parallel plate RF system, using a validated finite element computer model. The factors investigated were sample size, shape, relative position between the RF electrodes, and dielectric properties (DPs) of the sample and the surrounding medium. Effects of electrode gap and top electrode configuration on the RF power distribution behavior of the sample were also studied. The RF power uniformity in the samples was compared using RF power density uniformity index (PUI). Simulated results showed that the RF power uniformity in cuboid shaped samples, placed on the bottom electrode, first decreased and then increased with the increase in sample size. The sample shape and its vertical position between the fixed gap parallel plate electrodes also affected the RF power distribution and uniformity. A cuboid sample had higher RF power densities at the edges, while an ellipsoid had higher power densities in the center parts. Simulated results showed that the smaller values of DPs resulted in better RF power uniformities in the samples. Reducing the electrode gap improved the RF power uniformity of the sample. While studying the influence of the top electrode configuration on the RF power distribution and uniformity, the results showed that optimum RF power uniformity in a particular sample size could be achieved with a particular top electrode bending position and angle. The results are useful in understanding complex RF heating, designing and scaling up of efficient RF systems.

1. Introduction

Radio frequency (RF) technology has been explored in various food processing operations, such as pasteurization and sterilization (Bengtsson et al., 1970; Houben et al., 1991; Brunkhorst et al., 2000; Luechapattanaporn et al., 2005; Lagunas-Solar et al., 2005, 2007; Byrne et al., 2010) and insect disinfestations in various agricultural commodities, such as fresh fruits (Birla et al., 2004, 2005; Wang et al., 2006; Tiwari et al., 2008) and dry nuts (Wang et al., 2001, 2002, 2003, 2005, 2008b). A major obstacle for RF technology to be commercially applicable is its non uniform heating. Different factors, such as sample dielectric properties (DPs), size, shape, its position between the RF electrodes, and the electrode configuration may affect temperature uniformity in a RF treated food product. Barber (1983) reported that the temperature uniformity could be improved if electrodes are shaped to fit the surface of the material. Wang et al. (2005) observed temperature non-uniformity in in-shell walnuts, placed at different locations inside a 12 kW, 27.12 MHz RF system after 3 min of heating. Effect of three sample shapes (cube, cylinder, and sphere) on the temperature uniformity of meat has been simulated by Romano and Marra (2008). They reported that cubes should have a better temperature uniformity compared to cylinders and spheres. Birla et al. (2008a) reported a difference in temperature profiles of a model fruit when it was placed at different vertical and horizontal positions between the fixed gap RF electrodes. Simulation on the RF heating of meshed potato, conducted by Wang et al. (2008a) showed that the DPs of mashed potato and surrounding water affected heating rate and temperature distribution. Birla et al. (2008b) showed that the DPs of different constitutional parts (peel and pulp) of a fruit influenced its final temperature distribution after the RF heating. Petrescu and Ferariu (2008) reported the effect of the vertical gap between the RF electrodes, and the horizontal distance between the successive pair of electrodes on the heating uniformity of a dielectric material kept inside a staggered RF applicator. Wang et al. (2010) used three different electrode gaps to select the most suitable heating time for the RF heat treatment of lentils. Keeping the complexity of RF heating behavior in mind, a complete investigation on the RF heating behavior is essential to improve temperature distributions in treated food products.

Experimental methods are time consuming, costly, and often provide limited information. Computer simulation can be used as

* Corresponding author. Address: 213 LJ Smith Hall, Pullman, WA 99164-6120, USA. Tel.: +1 509 335 2140; fax: +1 509 335 2722.
E-mail address: jtang@wsu.edu (J. Tang).

0260-8774/$ - see front matter © 2011 Elsevier Ltd. All rights reserved.
doi:10.1016/j.jfoodeng.2011.01.015

an effective tool for rapid, cheap, flexible analysis, and for providing an insight into the RF heating mechanism in food materials. Computer simulation has previously been used to study the RF heating uniformity in various food materials, such as fresh fruits (Birla et al., 2008a,b), meat (Marra et al., 2007; Rayner, 2007; Romano and Marra, 2008), grain seeds (Yang et al., 2003), mashed potato (Wang et al., 2008a), and carboxy methyl cellulose solution (Chan et al., 2004). In our companion paper (Tiwari et al., 2011), we developed and validated a finite element based computer model for the RF heating of dry food products using wheat flour as a representative material. The simulation results, in that study, demonstrated that non-uniform distribution of the RF power density (which acted as a heat source) is mainly responsible for temperature non-uniformity in wheat flour. Therefore, as a starting step, it was important to access and study the behavior of the RF power density inside a dry product as influenced by important factors, such as sample size, shape, position, DPs, electrode gap, and top electrode configuration.

In the past, different criteria and indexes have been used to study, evaluate, and compare the RF power and temperature uniformity in food samples. Neophytou and Metaxas (1998) used normalized RF power density to compare the RF power uniformities in rapeseeds and raw potatoes. The temperature uniformity of walnuts, soybeans, wheat, and lentils has been experimentally assessed and compared by using a heating uniformity index, defined as the ratio of the difference in standard deviation rises to average sample temperature rises during the RF treatments (Wang et al., 2005). Romano and Marra (2008) compared the simulated average, maximum, and minimum temperatures of meat samples in three different shapes (cube, cylinder and sphere). In the present work, the RF power densities in dry food samples are accessed and compared under different conditions, using a simulated power uniformity index (PUI). The overall objective of the study was to help design and scale up efficient RF systems for industrial applications. Specific objectives of this study were to investigate the effect of (1) sample size, shape, and its relative vertical position between the electrodes, (2) sample and surrounding materials, and (3) electrode gap and top electrode configuration on the sample RF power density distribution.

2. Material and methods

2.1. Governing equations

2.1.1. RF power density and Laplace equations

When a dielectric material is placed between two plate RF electrodes, the local RF power density (Q , W m^{-3}) in the material is defined as:

$$Q = 2\pi f \varepsilon_o \varepsilon''_m |\boldsymbol{E}|^2 \quad (1)$$

where f is the frequency (Hz), ε_o and ε''_m are the permittivity of the free space (8.86×10^{-12} F m^{-1}), and the loss factor of the material, respectively. $|\boldsymbol{E}|$ is the modulus of electric field (V m^{-1}). Electric field ($\boldsymbol{E}$) inside the RF applicator is defined as the negative gradient of the electric voltage ($\boldsymbol{E} = -\nabla V$).

Quasi-static electric field approximation of Maxwell equation is used in the modeling of RF heating of dry food materials (Tiwari et al., 2011). Maxwell equation with quasi static electric field approximation is given by:

$$\nabla(\sigma + j * 2\pi f \varepsilon_o \varepsilon_m)\nabla V = 0 \quad (2)$$

where $j = \sqrt{-1}$, σ and ε_m are electrical conductivity (S m^{-1}) and complex relative permittivity of the material, respectively. The complex relative permittivity ε_m of the material is related to the dielectric constant ε'_m and loss factor ε''_m ($\varepsilon_m = \varepsilon'_m - j * \varepsilon''_m$).

2.1.2. Average RF power density and RF power uniformity index (PUI) of the sample

Average RF power density (Q_{av}, W m^{-3}) in a dielectric material is defined as the volume integral of the RF power density (Q, W m^{-3}) divided by material volume (V_{vol}, m^3):

$$Q_{av} = \frac{1}{V_{vol}} \int_{V_{vol}} Q \, dV_{vol} \quad (3)$$

RF power uniformity index (PUI) in a dielectric material is defined as:

$$\mathrm{PUI} = \frac{\frac{1}{V_{vol}} \int_{V_{vol}} sqrt((Q - Q_{av})^2) dV_{vol}}{Q_{av}} \quad (4)$$

It is clear from Eq. (4) that PUI should be smaller for better RF power uniformity in the dielectric material. The minimum value of PUI is zero, which indicates uniform RF power in dielectric material. A well designed RF system should have a low PUI.

2.2. Physical and simulation model

A 12 kW, 27.12 MHz RF system (Strayfield Fastran with E-200, Strayfield International Limited, Wokingham, UK) was used as a physical model. The description of RF system can be found elsewhere (Birla et al., 2008a,b; Tiwari et al., 2011). It was not feasible to include every single detail of the RF system in simulations due to excessive time and computer resource requirements. Therefore, only a quarter part of the symmetric RF system was simulated. Fig. 1 shows the RF cavity geometry, boundary conditions, and the coordinate system used in simulation.

2.3. DPs of sample and surrounding medium

Tiwari et al. (2011) measured the DPs of wheat flour within the temperature range of 20–70 °C. Average DPs ($3.78 - j * 0.33$) of wheat flour were used in all simulations, except for the cases in which the effect of the sample DPs on the RF power uniformity was investigated. Similarly, air ($1 - j * 0$) was used as a surrounding material in all simulations, except for the cases in which the effect of the surrounding material dielectric constants on the RF power uniformity was investigated.

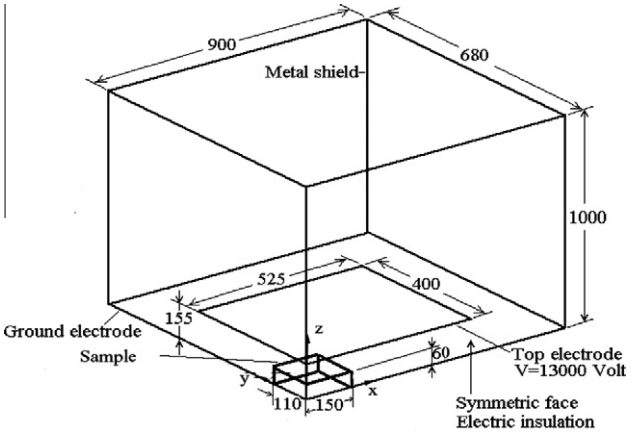

Fig. 1. Geometrical and boundary conditions of one quadrant of a 12 kW, 27.12 MHz radio frequency system (dimensions are in mm). Diagram is not drawn to the scale.

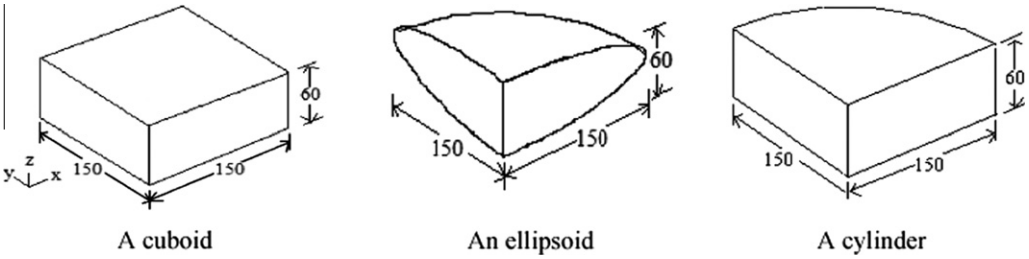

Fig. 2. Dimensions (in mm) of the cuboid, the ellipsoid, and the cylinder used in simulations.

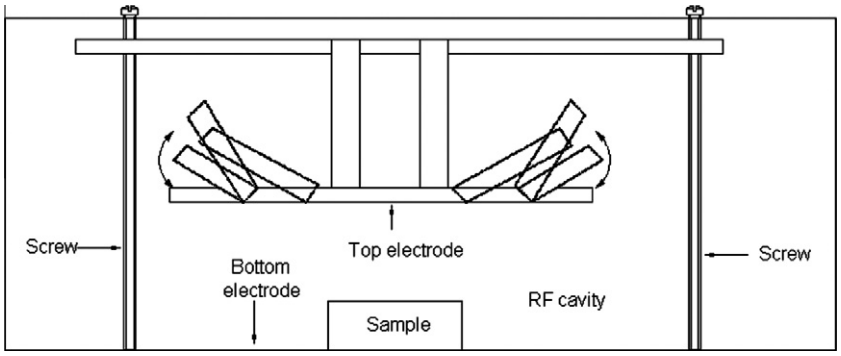

Fig. 3. Schematic diagram of radio frequency cavity showing change in top electrode configuration by bending it upward from its both ends at different lengths and angles.

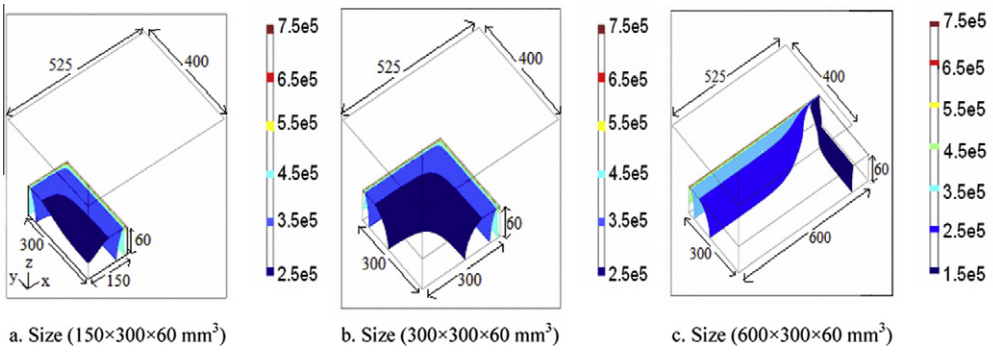

Fig. 4. Simulated power uniformity indexes (PUIs) in wheat flour sample with three different sizes, placed on the bottom electrode with a fixed electrode gap of 155 mm. Top electrode size was 525 × 400 mm^2.

2.4. Boundary conditions

Constant electrical voltage (13,000 V) was applied on the top electrode (Tiwari et al., 2011). Since the bottom electrode was grounded and attached to the metallic casings of the RF cavity, voltage (0 V) was assigned to all metallic casings and to the bottom electrode. Electrical insulation ($\nabla E = 0$) boundary condition was assigned to the symmetrical faces of RF applicator and the sample.

2.5. Simulation methodology

Commercially available finite element based software FEMLAB (V3.4, COMSOL Multiphysics, Burlington, MA, USA) was used for simulations. Inbuilt AC/DC module with quasi-static analysis was selected to solve Maxwell equation. In each simulation, model geometry was first constructed and meshed. A relatively fine mesh was generated at the interface of the sample and the surrounding medium. Linear system solver (UMFPACK) was used to solve the partial differential equation (Eq. (2)). Once the solution was obtained, average RF power density (Q_{av}) and PUI of the sample (Eqs. (3) and (4)) were calculated using FEMLAB inbuilt integration scheme. The mesh system was refined again and solved for a new set of average RF power density (Q_{av}) and PUI of the sample. The newly obtained sample PUI was compared with that at the previous step. The process was repeated until the sample PUI (Eq. (4)) in the successive mesh refinement did not change to the third decimal point. Solution time for each simulation varied between 20 and 60 min, depending on the sample and mesh size. All simulations were performed on a Dell 670 workstation with two Dual-Core, 2.80 GHz XEON processors and 12 GB RAM running a Windows XP 64-bit operating system.

2.6. Simulation sequence

2.6.1. Simulation with varying sample size, position and shape

Wheat flour samples shaped in cuboids were placed on the ground electrode. A series of simulations were run by changing lengths and widths of samples progressively at regular intervals between 50 and 600 mm, while the height was fixed as 60 mm. Another set of simulations were performed by varying the sample

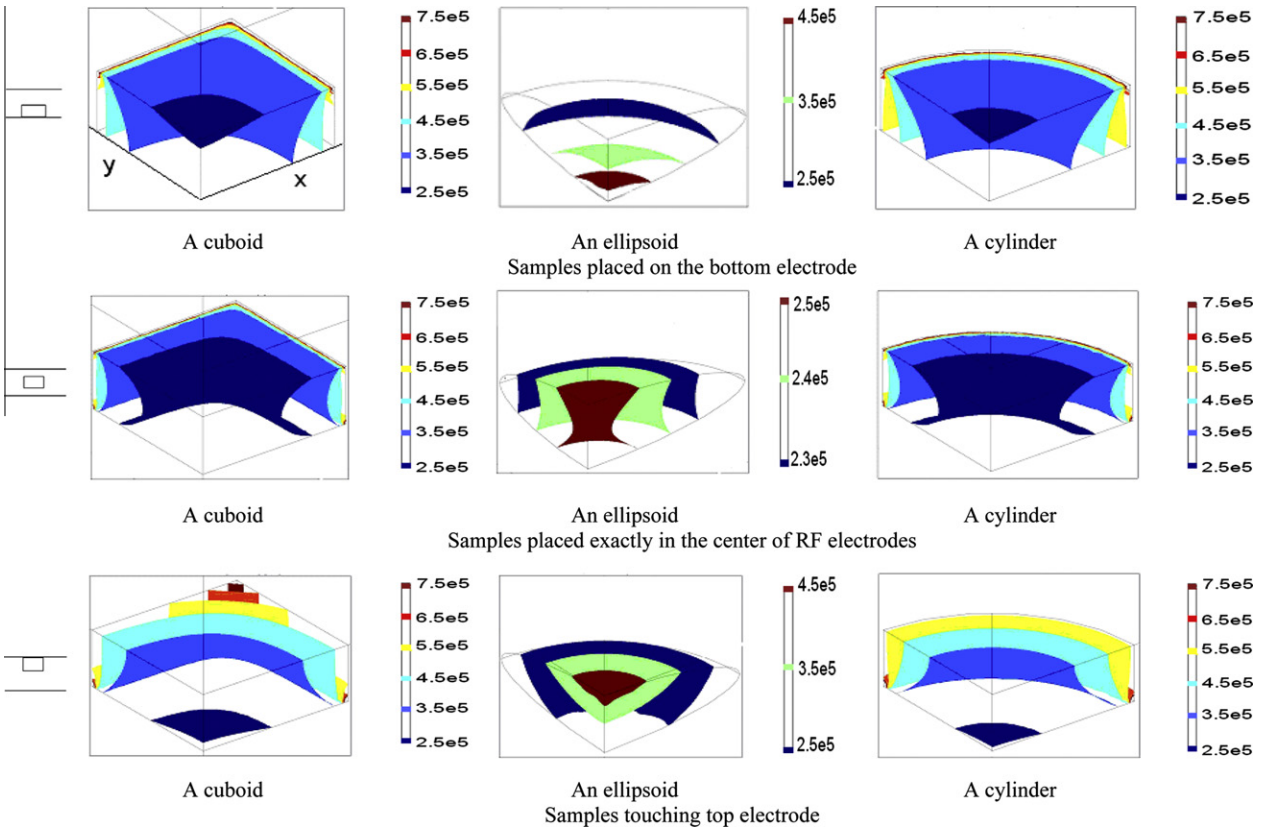

Fig. 5. Simulated RF power density contours (W m^{-3}) of wheat flour sample in three different shapes (a cuboid, an ellipsoid, and a cylinder) placed at three different vertical positions between the RF electrodes of fixed gap of 155 mm.

heights ranging between 10 and 100 mm with lengths and widths fixed at 150 mm. The electrode gap in each simulation was set at 155 mm. Trends of the RF power density distribution and PUIs of flour in each simulation were determined.

Based on previous simulation results, three cuboids ($50 \times 50 \times 60$ mm^3, $150 \times 150 \times 60$ mm^3, $300 \times 300 \times 60$ mm^3) were selected to study the effect of sample vertical position between the fixed gap of the RF electrodes. The selected cuboids corresponded to small, medium, and large sample sizes, and the dimensions represented lengths, widths, and heights of cuboids along x, y and z axes as shown in Fig. 1. The top and the bottom electrode positions were fixed at $z = 0$ and $z = 155$ mm, measured from the bottom electrode but the load vertical positions were changed between the fixed gap (155 mm) of the RF electrodes. The cuboids were placed at seven vertical positions ($z = 0$, 17.5, 37.5, 47.5, 57.5, 77.5, and 95 mm) from the bottom electrode. Positions ($z = 0$, 47.5, and 95 mm) were the vertical elevations when the samples were placed on the bottom electrode, exactly in the middle of the RF electrodes and in touch with the top electrode. Positions ($z = 17.5$, 37.5, 57.5 and 77.5) were the vertical elevations in which the samples were placed at equal distances (−30, −10, +10 and +30 mm) from the central position. Trends of RF power density distribution with PUIs were determined in each simulation.

A cuboid, an ellipsoid, and a cylinder were chosen to study the effect of container shape. Dimensions of shapes were considered as $150 \times 150 \times 60$ mm^3, which represented length, width, and height in the cuboid, equatorial radiuses and height in the ellipsoid and two mutually perpendicular radiuses and height in the cylinder along x, y and z directions, respectively (Fig. 2). The samples were placed at three different vertical positions: on the ground electrode, in the middle of the electrodes, and in contact with the top electrode. RF power density contours and PUIs of the samples were determined and reported for each simulated scenario.

2.6.2. Simulation with varying DPs of the sample and surrounding medium

To study the effect of the DPs on the sample PUI, simulations were run by changing dielectric constant of the sample from 1 to 100, for various loss factors ranging between 0.5 and 100. A cuboid sample ($150 \times 150 \times 60$ mm^3) was placed on the ground electrode with an electrode gap of 155 mm. Another set of simulations were performed in three different sized cuboids with a narrowed range of dielectric constant (6–14) for a set loss factor of 10. The surrounding material dielectric constant was also varied between 1 and 30 with a set sample DPs ($8 - j * 10$) to study the effect of the surrounding material dielectric constant on PUI. Sample DPs were selected, based on the previous simulation results as explained in Section 3.5.

2.6.3. Simulation with varying electrode gap and top electrode configuration

Simulations were run by changing the top electrode position between 65 mm and 155 mm, while a cuboid sample ($150 \times 150 \times 60$ mm^3) was kept on the ground electrode. The electrode gap was changed by varying the position of the top electrode. Tiwari et al. (2011) demonstrated that edge heating inside a rectangular container was mainly due to an increased electric field concentration at the corners and at the edges. Therefore, it was hypothesized that bending the top electrode upward should reduce the electric field strength in these parts and improve the heating uniformity of the sample. A schematic diagram of the RF cavity with the top electrode bending at different positions and

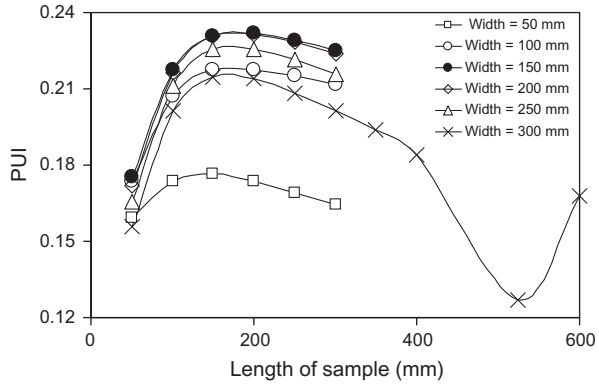

Fig. 6. Simulated RF power uniformity indexes (PUIs) of cuboid shaped wheat flour mass with varying sample lengths and widths. Cuboids were placed on the bottom electrode with top electrode size ($525 \times 400\ mm^2$) and a fixed electrode gap of 155 mm. Sample heights were set as 60 mm.

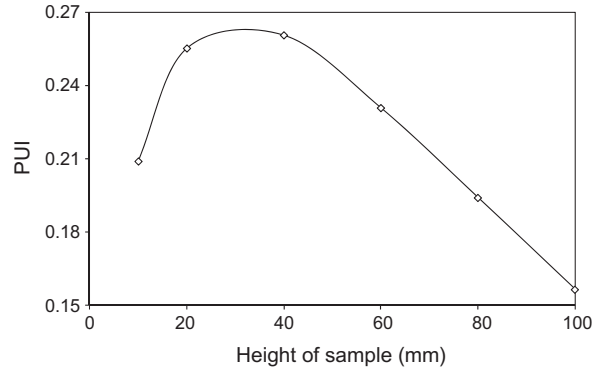

Fig. 7. Simulated RF power uniformity indexes (PUIs) of cuboid shaped wheat flour with varying sample heights. Samples were kept on the bottom electrode with a fixed electrode gap of 155 mm. Top electrode size was $525 \times 400\ mm^2$ and samples length and width both were set as 150 mm.

angles is shown in Fig. 3. The top electrode was bent upward from its both ends at different lengths and angles. Firstly, simulations were run for different bending positions (0, 100, 200, 300, 400, 500 mm) measured from the center of the electrode. Bending angles in all these simulations were set as 15°. Secondly, angles were varied between 0° and 90°, with the bending position fixed as 200 mm. In all simulations, a cuboid sample ($300 \times 210 \times 60\ mm^3$) was placed on the ground electrode.

3. Results and discussions

3.1. Distribution of RF power density in different sample sizes

Fig. 4 shows the general trends of RF power density distribution of wheat flour in three different cuboids, placed on the ground electrode. The cuboids were selected in such a way that two cuboids ($150 \times 300 \times 60\ mm^3$, $300 \times 300 \times 60\ mm^3$) were completely inside the RF electrodes. The cuboid ($600 \times 300 \times 60\ mm^3$) was partially inside the RF electrodes, as the top electrode size was $525 \times 400\ mm^2$. The two low RF power density contours, $2.5 \times 10^5\ W\ m^{-3}$ and $3.5 \times 10^5\ W\ m^{-3}$ (shown in navy blue[1] and light blue color), were at the inner parts of the samples. The four higher RF power density contours, 4.5×10^5, 5.5×10^5, 6.5×10^5, and $7.5 \times 10^5\ W\ m^{-3}$ (shown in cyan, yellow, red, and brown color),

[1] For interpretation of color in Figs. 4, 5 and 11, the reader is referred to the web version of this article.

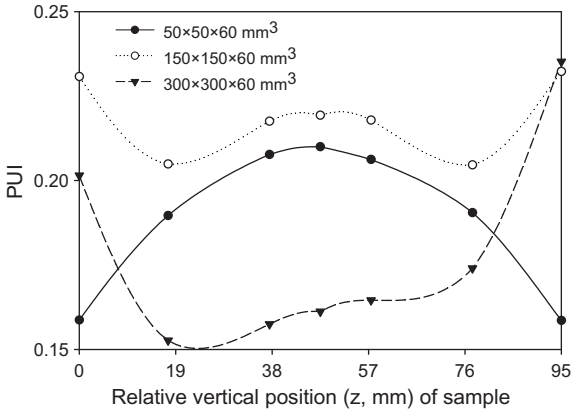

Fig. 8. Simulated power uniformity indexes (PUIs) of cuboid shaped wheat flour in three different sizes, kept at seven different vertical positions (along *z* axis) under the fixed electrode gap of 155 mm. Coordinate system was shown in Fig. 1.

Table 1
Simulated PUIs of wheat flour sample in three different shapes (a cuboid, an ellipsoid, and a cylinder), placed at three different vertical positions between RF electrodes with a fixed gap of 155 mm.

Sample shape	Relative position of sample	Simulated PUI
A cuboid ($150 \times 150 \times 60\ mm^3$)	Touching bottom electrode	0.23
	In the center of RF electrodes	0.22
	Touching top electrode	0.23
An ellipsoid ($150 \times 150 \times 60\ mm^3$)	Touching bottom electrode	0.16
	In the center of RF electrodes	0.06
	Touching top electrode	0.16
A cylinder ($150 \times 60\ mm^3$)	Touching bottom electrode	0.22
	In the center of RF electrodes	0.22
	Touching top electrode	0.22

were at the edges of the sample (Fig. 4a and b). Thus, the RF power densities increased from inner to outer parts in the first two cuboids. Higher RF power densities, occurred at the edges compared to the other parts, indicated edge heating in these samples. It was also noticeable that relative sample volumes containing the same RF power density contours were more in $300 \times 300 \times 60\ mm^3$ (Fig. 4b) than in $150 \times 300 \times 60\ mm^3$ (Fig. 4a), which indicated that the sample size affected the RF power uniformity, which was explained in detail in Section 3.3. RF power density distribution was different for the third sample (Fig. 4c), where edge heating occurred only when the sample dimension was less than that of the electrodes. RF power densities close to that edge were between 4.5×10^5 and $7.5 \times 10^5\ W\ m^{-3}$ (contours are shown in green, yellow, red, and brown color). The other edge and the sample section which was outside the RF electrodes had the lowest RF power densities. Fig. 4c shows that RF power density contour at the outer most section was $1.5 \times 10^5\ W\ m^{-3}$ (shown in navy blue color), while RF density contours at the sample inner sections were $2.5 \times 10^5\ W\ m^{-3}$ and $3.5 \times 10^5\ W\ m^{-3}$ (shown in light blue and cyan color).

The difference in RF power density patterns in the different sample sizes can be explained by the behavior of electric field. When wheat flour samples were put completely between the RF electrodes, electric field, deflected by the edges and corners increased the net electric field at the outer sections compared to the inner sections of the samples (Marra et al., 2007; Birla et al., 2008a; Tiwari et al., 2011). Since RF power density is proportional to the square of electric field, it also increased from inner to outer sections of the samples. In case of the third sample, net electric

field was comparatively smaller at the outer-most sections of the sample as the sample was larger than the electrode size. That is why, RF power density increased and then decreased from the inner to outer sections of third sample.

3.2. Distribution of RF power density in different sample shapes, placed in different positions between the RF electrodes

It is also desirable to investigate the effect of sample shapes (a cuboid, a cylinder and an ellipsoid) on the RF power density distribution as most of the dry agricultural commodities such as grains, food powders, spices, and dry fruits are kept either in boxes, cans, or in pouches. Fig. 5 shows the general trends of RF power density distribution in the cuboid, ellipsoid, and cylinder, kept at three different positions. It was clear that cuboid and cylinder had higher RF power densities at their outer parts as the RF power density contours, 4.5×10^5, 5.5×10^5, 6.5×10^5, and 7.5×10^5 W m^{-3} (shown in green, yellow, red, and brown color), were close to the edge of the samples, while the two lower RF power density contours, 2.5×10^5 W m^{-3} and 3.5×10^5 W m^{-3} (shown in navy blue and light blue color), were at the inner parts of the samples. Trends of RF power density distribution were opposite in the ellipsoid, where higher RF power densities were at its inner parts of the samples. The highest RF power density contour 4.5×10^5 W m^{-3} (shown in brown color) and the lowest RF power density contour was close to the central and peripheral parts of the ellipsoid, respectively. In the cuboid and cylinder, electric field is deflected by the sample edges, resulted in increase of net electric field concentration at the outer sections of the samples; while in ellipsoid, electric field was deflected by every point located on its curved surface. As a result, net electric field concentration at the inner sections was higher compared to that of outer sections of the sample.

RF power density patterns in samples also changed with sample placement between the electrodes. Sample in contact with either of the electrodes had higher RF power densities near the contact surfaces due to increased electric field concentration at the contact surfaces. Samples placed in the middle of RF electrodes showed higher RF power densities at their central sections as electric field deflected by both (top and bottom) edges increased net electric field concentration at the central parts of the sample.

3.3. Effect of sample size on PUI

Figs. 6 and 7 summarize the effect of sample size on PUI of wheat flour. Simulated results demonstrated that increase in sample length and width caused initial increase and then the reduction of PUI (Fig. 6). Values of PUI were the highest when sample lengths and widths lied between 150 and 200 mm, 35–50% of the top electrode size (525 × 400 mm^2). Since patterns of PUI change were similar with respect to lengths and widths, only lengths were varied in later simulations. PUI was the lowest when the sample length was equal to the electrode length (525 mm). Increase in the sample length beyond the electrode length increased PUI. Similarly, when the sample height was increased, PUI decreased after showing initial increase (Fig. 6). It is clear form Figs. 6 and 7 that the RF power uniformity should be better for sample sizes, either approaching zero or approaching the maximum possible size that can be kept completely between the RF electrodes.

When sizes approached to zero, the major part of the electric field passed directly through the ground electrode, without entering into samples. Because of that, RF power was more uniform in small samples, as indicated by low PUIs. With increase in sizes, more electric field started entering into the samples. At first, most of the electric field entered obliquely as sizes were comparatively smaller than those of the top electrode size. Oblique electric field

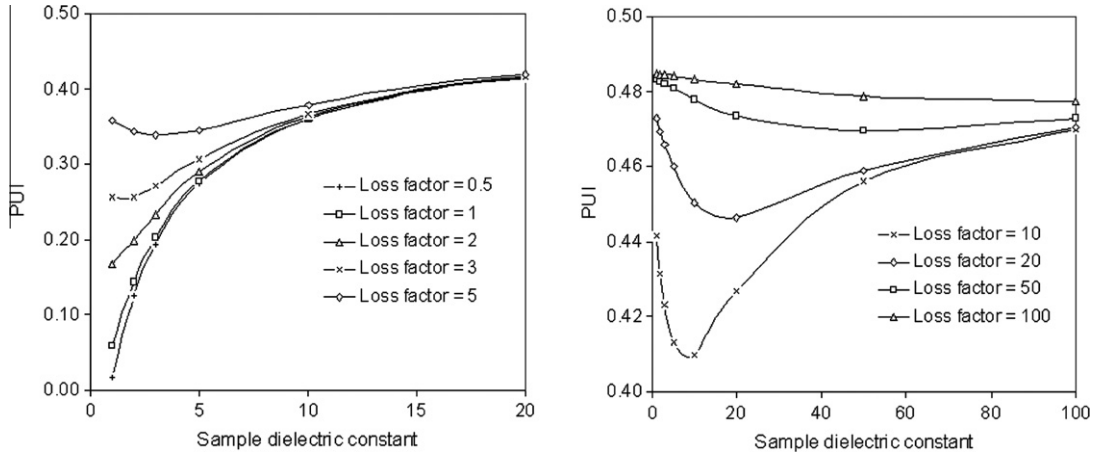

Fig. 9. Simulated power uniformity indexes (PUIs) in cuboid shaped sample (150 × 150 × 60 mm^3) with varying DPs. Samples were placed on the bottom electrode with an electrode gap of 155 mm.

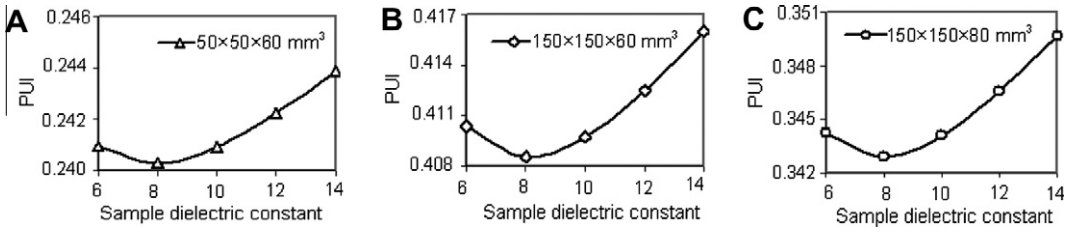

Fig. 10. Trends of simulated power uniformity indexes (PUIs) of samples with varying dielectric constants in three different size cuboids. Loss factor value was fixed as 10.

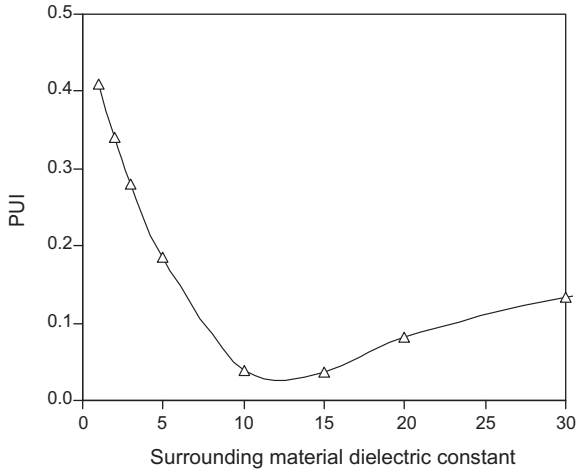

Fig. 11. Simulated power uniformity indexes (PUIs) in sample ($150 \times 150 \times 60\ mm^3$) in different surrounding medium dielectric constants. Sample DPs was fixed as $(8 - 10 * j)$ and it was kept on the bottom electrode with an electrode gap of 155 mm.

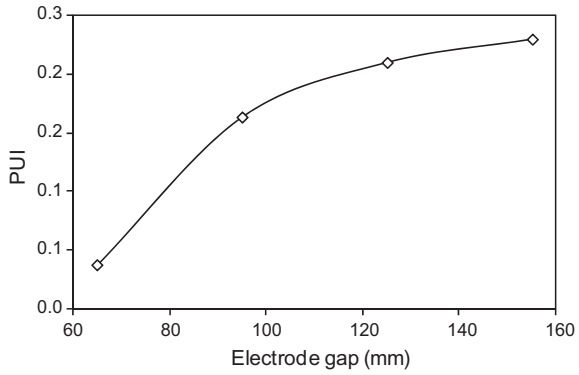

Fig. 12. Simulated power uniformity indexes (PUIs) of cuboid shaped wheat flour ($150 \times 150 \times 60\ mm^3$) with varying electrode gaps. Sample was kept on the bottom electrode.

increased the RF power non-uniformities in samples. With a further increase in sample size, the electric field started entering normally (except a small area, which was getting deflected by sample edges and corners) into the sample. This caused increase in the RF power uniformity again.

3.4. Effect of sample vertical position on PUI

Fig. 8 shows the effect of sample vertical position on PUI. Three sample sizes were selected based on the results explained in Fig. 6. These sizes could be considered as small, medium, and big compared to top electrode size. It is clear from Fig. 8 that trends of PUI change depended on the sample sizes as well as their relative vertical positions between the RF electrodes. For the samples of size $50 \times 50 \times 60\ mm^3$, PUI increased and then decreased when a sample was moved up from the bottom to the top electrode. PUI change was symmetrical around the central ($z = 47.5$ mm) position, with its highest value at this position. In sample size ($150 \times 150 \times 60\ mm^3$) unlike size ($50 \times 50 \times 60\ mm^3$), PUIs were the highest when samples were placed on the bottom electrode ($z = 0$ mm) or in touch with the top electrode ($z = 95$ mm). PUI change was symmetrical around the central ($z = 47.5$ mm) position. For the sample size ($300 \times 300 \times 60\ mm^3$), PUI change was not symmetric around the central position. After initial decrease of PUI when moved from $z = 0$ to 17.5 mm, sample PUI continued to increase when it was moved toward top electrode. Ideally, PUI change should be symmetrically distributed around the central position, but the simulated results showed that it was not true in the case of large samples. The reason could be attributed to the unequal sizes of the top and the bottom electrodes. The bottom (grounded) electrode was the integral part of RF cavity with no open edges, where as the top electrode had open edges. Electric field distribution near the open edges of the top electrode must have affected the RF power uniformity of big sample sizes, when they were moved closer to the top electrode. Based on the results, it could be concluded that the RF power should be more uniform in the small samples if they are placed either in contact with the top or the bottom electrode but for middle and large size samples, better RF power uniformity can be achieved in carefully selected positions between the RF electrodes.

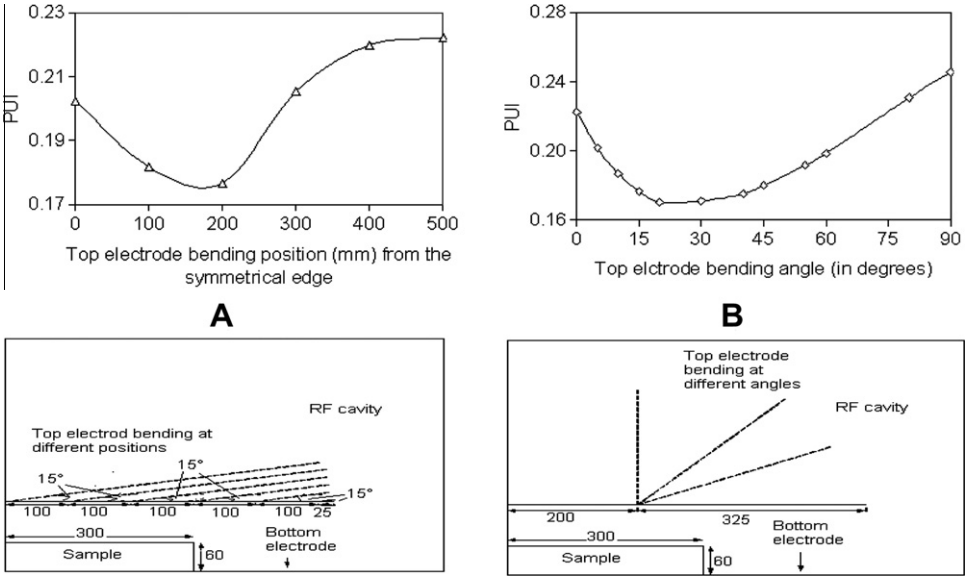

Fig. 13. Simulated power uniformity indexes (PUIs) in a cuboid shaped wheat flour ($300 \times 210 \times 60\ mm^3$) sample, placed on the bottom electrode when top electrode ($525 \times 400\ mm^2$) was bent (A) at six different positions (0, 100, 200, 300, 400 and 500 mm) along the length of electrode, keeping bending angle fixed as 15°, and (B) at different angles (in degrees), keeping bending position fixed as 200 mm.

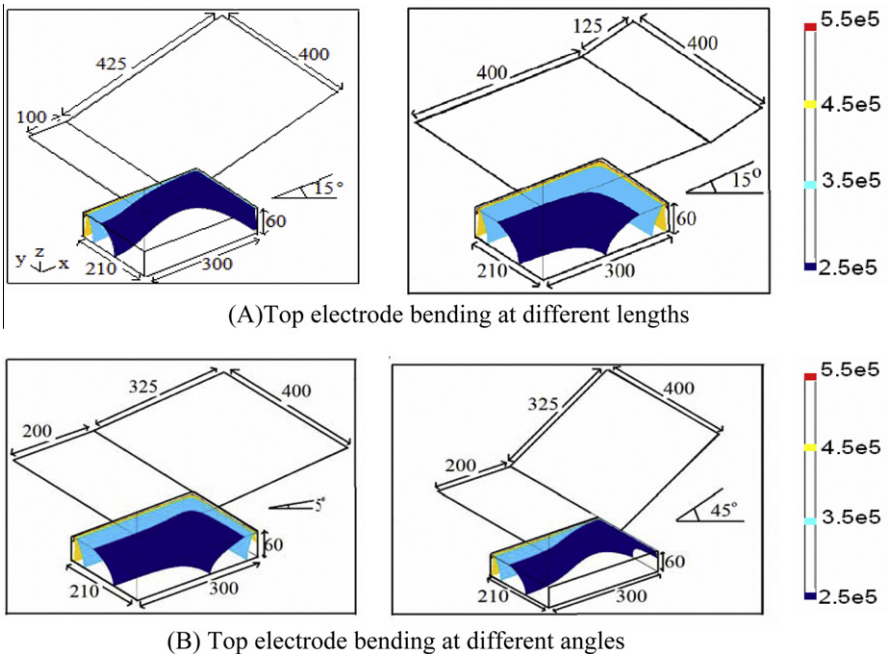

Fig. 14. Simulated power density contours (W m^{-3}) in a cuboid shaped wheat flour sample (300 × 210 × 60 mm^2) placed on the bottom electrode, when top electrode (525 × 400 mm^2) was (A) bent 100 and 400 mm along the length of electrode, keeping bending angle fixed as 15° and (B) bent upwards 5° and 45°, keeping bending position fixed as 200 mm.

Table 1 compares the simulated PUIs of the cuboid, ellipsoid and cylinder, placed at three different vertical elevations. PUIs were the lowest in the ellipsoid, followed by the cylinder and cuboid for all the three positions. Ellipsoid placed in the center of the RF electrodes had the lowest PUI among all the selected positions.

3.5. Effect of DPs of sample and surrounding medium on sample PUI

Fig. 9 indicates that the smaller DPs resulted in better RF power uniformities in the samples. Dry products should provide a better uniform RF heating because of the smaller DPs. It was also observed if loss factor was $\leqslant 1$, PUI continued to increase with the increase in dielectric constant. But for the loss factor >1, PUIs first decreased and then increased with the increase in dielectric constant. It was interesting to notice that PUIs had their minimum values whenever the dielectric constants were about the same as the loss factors, though this was more discernable for the smaller DPs. Results in Fig. 10 show that trends of PUI change were independent of the sample sizes. PUI first decreased and then increased between the dielectric constants 6 and 14, showing its minimum at a dielectric constant value of 8 when the loss factor was 10. Fig. 11 shows the effect of the surrounding material dielectric constant on PUI. The sample DPs were set as $(8 - j * 10)$, based on the previous simulations. PUI first decreased and then increased with the increase in the surrounding material dielectric constant. PUI was the lowest when the surrounding material dielectric constant was between 10 and 15. From the results, it is clear that the RF uniformity can be achieved when the surrounding material dielectric constant is in a comparable range of the sample DPs.

3.6. Effect of electrode gap on PUI

PUI of wheat flour decreased as the electrode gap was reduced from 155 to 65 mm, as shown in Fig. 12. As explained earlier, a proportion of oblique electric field, which caused the RF power non-uniformity decreased when the electrode gap was reduced.

3.7. Effect of top electrode bending/configuration

Fig. 13A shows the effect of the top electrode bending position on the sample PUI. The results demonstrated that the top electrode bending position greatly affected the sample PUI. When the top electrode was bent at 200 mm from the center of the electrode, PUI was lower compared to when it was bent at the other five positions. Similarly, Fig. 13B shows the effect of the top electrode bending angle on the PUI of wheat flour sample. Increase in bent angle, first decreased and then increased PUI. Sample PUI was the lowest at bent angle 20°. The RF power density distribution contours in two different positions and angles are shown in Fig. 14. It is clear that the top electrode bending affected the RF power density distribution inside the wheat flour sample as the RF power density contours 2.5×10^5, 3.5×10^5, 4.5×10^5, and 5.5×10^5 W m^{-3} (shown in navy blue, cyan, yellow, and red color) had different distribution patterns in each scenario. Based on the above results it can be concluded that the top electrode configuration affected the RF power uniformity in the sample as magnitudes of the electric fields and their distributions inside the wheat flour sample changed with the top electrode bending positions and angles. Optimum RF power uniformity in a particular sample size could be achieved with a particular top electrode bending position and angle.

4. Conclusions

Effects of various factors such as sample size, shape, its relative position between the RF electrodes, top electrode configuration, and the DPs of sample and surrounding medium on the RF heating of a low loss factor food material placed inside a 27.12 MHz RF system were studied using a developed finite element computer model in FEMLAB 3.4. Simulated results showed that the RF heating uniformity could be improved using larger sample sizes placed in the air between the RF electrodes. Cubes and cylinders showed edge heating while ellipsoids showed center heating. Simulated results also showed that the smaller DPs provided better RF power uniformities in the material. Top electrode bending (bent position

and angle) affected the RF heating uniformity in the sample. The study helped understand the RF heating process, influenced by various parameters. The developed model is a very effective tool to design the RF electrode configuration and to obtain a better heating uniformity.

References

Barber, H., 1983. Electroheat, first ed. Granada Publishing Limited, London.

Bengtsson, N.E., Green, W., Valle, F.R.D., 1970. Radio frequency pasteurization of cured hams. Journal of Food Science 35 (5), 682–687.

Birla, S.L., Wang, S., Tang, J., 2008a. Computer simulation of radio frequency heating of model fruit immersed in water. Journal of Food Engineering 84 (2), 270–280.

Birla, S.L., Wang, S., Tang, J., Fellman, J.K., Mattinson, D.S., Lurie, S., 2005. Quality of oranges as influenced by potential radio frequency heat treatments against Mediterranean fruit flies. Postharvest Biology and Technology 38 (1), 66–79.

Birla, S.L., Wang, S., Tang, J., Hallman, G., 2004. Improving heating uniformity of fresh fruit in radio frequency treatments for pest control. Postharvest Biology and Technology 33 (2), 205–217.

Birla, S.L., Wang, S., Tang, J., Tiwari, G., 2008b. Characterization of radio frequency heating of fresh fruits influenced by dielectric properties. Journal of Food Engineering 89 (4), 390–398.

Brunkhorst, C., Ciotti, D., Fredd, E., Wilson, J.R., Geveke, D.J., Kozempel, M., 2000. Development of process equipment to separate nonthermal and thermal effects of RF energy on microorganisms. Journal of Microwave Power and Electromagnetic Energy 35 (1), 44–50.

Byrne, B., Lyng, J.G., Dunne, G., Bolton, D.J., 2010. Radio frequency heating of comminuted meats – considerations in relation to microbial challenge studies. Food Control 21 (2), 125–131.

Chan, T.V.C.T., Tang, J., Younce, F., 2004. 3-Dimensional numerical modeling of an industrial radio frequency heating system using finite elements. Journal of Microwave Power and Electromagnetic Energy 39 (2), 87–105.

Houben, J., Schoenmakers, L., Vanputten, E., Vanroon, P., Krol, B., 1991. Radiofrequency Pasteurization of Sausage Emulsions as a Continuous Process. Journal of Microwave Power and Electromagnetic Energy 26 (4), 202–205.

Lagunas-Solar, M.C., Pan, Z., Zeng, N.X., Truong, T.D., Khir, R., Amaratunga, K.S.P., 2007. Application of radio frequency power for non-chemical disinfestation of rough rice with full retention of quality attributes. Applied Engineering in Agriculture 23 (5), 647–654.

Lagunas-Solar, M.C., Zeng, N.X., Essert, T.K., Truong, T.D., Pina, C., Cullor, J.S., Smith, W.L., Larrain, R., 2005. Disinfection of fishmeal with radiofrequency heating for improved quality and energy efficiency. Journal of the Science of Food and Agriculture 85 (13), 2273–2280.

Luechapattanaporn, K., Wang, Y.F., Wang, J., Tang, J.M., Hallberg, L.M., Dunne, C.P., 2005. Sterilization of scrambled eggs in military polymeric trays by radio frequency energy. Journal of Food Science 70 (4), E288–E294.

Marra, F., Lyng, J., Romano, V., McKenna, B., 2007. Radio-frequency heating of foodstuff: solution and validation of a mathematical model. Journal of Food Engineering 79 (3), 998–1006.

Neophytou, R.I., Metaxas, A.C., 1998. Combined 3D FE and circuit modeling of radio frequency heating systems. Journal of Microwave Power and Electromagnetic Energy 33 (4), 243–262.

Petrescu, C., Ferariu, L., 2008. Modeling of dielectric heating in radio-frequency applicator optimized for uniform temperature by means of genetic algorithms. World Academy of Science, Engineering and Technology 47, 129–134.

Rayner, M., 2007. Multi Physics modeling of radio frequency cooking. In: Excerpt from the Proceedings of the COMSOL Users Conference, Grenoble France.

Romano, V., Marra, F., 2008. A numerical analysis of radio frequency heating of regular shaped foodstuff. Journal of Food Engineering 84 (3), 449–457.

Tiwari, G., Wang, S., Birla, S.L., Tang, J., 2008. Effect of water-assisted radio frequency heat treatment on the quality of 'Fuyu' persimmons. Biosystems Engineering 100 (2), 227–234.

Tiwari, G., Wang, S., Tang, J., Birla, S.L., 2011. Computer simulation model development and validation of radio frequency (RF) heating of dry food materials. Journal of Food Engineering. doi:10.1016/j.jfoodeng.2011.01.016.

Wang, J., Olsen, R.G., Tang, J., Tang, Z., 2008a. Influence of mashed potato dielectric properties and circulating water electric conductivity on radio frequency heating at 27 MHz. Journal of Microwave Power and Electromagnetic Energy 42 (2), 31–46.

Wang, S., Birla, S.L., Tang, J., Hansen, J.D., 2006. Postharvest treatment to control codling moth in fresh apples using water assisted radio frequency heating. Postharvest Biology and Technology 40 (1), 89–96.

Wang, S., Ikediala, J.N., Tang, J., Hansen, J.D., Mitcham, E., Mao, R., Swanson, B., 2001. Radio frequency treatments to control codling moth in in-shell walnuts. Postharvest Biology and Technology 22 (1), 29–38.

Wang, S., Tang, J., Cavalieri, R.P., Davies, D.C., 2003. Differential heating of insects in dried nuts and fruits associated with radio frequency and microwave treatments. Transactions of the ASAE 46 (4), 1175–1182.

Wang, S., Tang, J., Johnson, J.A., Mitcham, E., Hansen, J.D., Cavalieri, R.P., Bower, J., Biasi, B., 2002. Process protocols based on radio frequency energy to control field and storage pests in in-shell walnuts. Postharvest Biology and Technology 26 (3), 265–273.

Wang, S., Tiwari, G., Jiao, S., Johnson, J.A., Tang, J., 2010. Developing postharvest disinfestation treatments for legumes using radio frequency energy. Biosystems Engineering 105 (3), 341–349.

Wang, S., Yue, J., Chen, B., Tang, J., 2008b. Treatment design of radio frequency heating based on insect control and product quality. Postharvest Biology and Technology 49 (3), 417–423.

Wang, S., Yue, J., Tang, J., Chen, B., 2005. Mathematical modeling of heating uniformity for in-shell walnuts subjected to radio frequency treatments with intermittent stirrings. Postharvest Biology and Technology 35 (1), 97–107.

Yang, J., Zhao, Y., Wells, J.H., 2003. Computer simulation of capacitive radio frequency (RF) dielectric heating on vegetable sprout seeds. Journal of Food Process Engineering 26 (3), 239–263.